Meas. Sci. Technol. **18** (2007) 3501–3510 doi:10.1088/0957-0233/18/11/034

Control of flux in magnetic circuits for Barkhausen noise measurements

Steven White[1], **Thomas Krause**[2] **and Lynann Clapham**[1]

[1] Department of Physics, Queen's University, Kingston, Ontario K7L 3N6, Canada
[2] Department of Physics, Royal Military College of Canada, PO Box 17000 Stn Forces, Kingston, Ontario K7K 7B4, Canada

Received 28 February 2007, in final form 23 August 2007
Published 4 October 2007
Online at stacks.iop.org/MST/18/3501

Abstract
The consistency of magnetic Barkhausen noise (MBN) measurements under applied sinusoidal magnetic field control and sinusoidal magnetic circuit flux control was investigated under variable circuit permeability conditions. A U-core electromagnet was used to provide the alternating magnetic excitation. The magnetic circuit permeability was changed by varying excitation magnet lift-off and by using samples with known magnetic anisotropy. By controlling the circuit magnetic flux, measured as the flux in one of the U-core poles near the sample, MBN measurements were found to be consistent and independent of the excitation magnet lift-off in both a Si–Fe steel sample and an interstitial free (IF) steel sample at peak sample flux densities greater than 1.16 T and 0.29 T respectively. Consistency within a 95% confidence level was demonstrated for lift-off values of 0.6 mm or less, with decreasing sensitivity to lift-off observed at higher fluxes. MBN anisotropy measurements were also performed using both field control and flux control. Under field control conditions a component of the anisotropy signal was found to be dependent on the magnetic circuit permeability. This permeability dependence was absent when using flux control. The results demonstrated that flux control should be used when performing MBN measurements on samples where lift-off may be an issue, as values obtained will have less dependence on the excitation magnet characteristics than when field control is used.

Keywords: magnetic Barkhausen noise, magnetic anisotropy, permeability

1. Introduction

Magnetic Barkhausen noise (MBN) is the result of abrupt local changes of magnetization in ferromagnetic materials as the domain structure reconfigures around pinning sites and domains are created and annihilated in response to a changing magnetic field [1, 2]. MBN is known to be affected by material microstructure, and is a candidate for non-destructive evaluation (NDE) applications due to its response to elastic stresses [3–15].

Over the last two decades a significant number of studies have revealed statistical dependencies of MBN on both the sample magnetization distribution and its rate, as domain reconfiguration processes vary at different points in the hysteresis cycle [16, 17]. In regions of the hysteresis loop where the differential permeability of the sample material is constant, power laws and scaling relationships have been observed [17–20], leading to discussion of self-organized criticality of MBN [18–21]. To obtain these fundamental results, however, ideally prepared samples wound with encircling coils have been used, and measurements have been performed over several hours [19] in order to individually distinguish Barkhausen events.

In NDE applications, measurements must be performed in a timely fashion on an engineering material, with an inexact history and geometry, and limited access. Typically, for surface Barkhausen measurements, a U-core electromagnet is placed in contact with the sample, and a pickup coil or read head is placed on the sample to sense the Barkhausen events. While potentially a sensitive NDE tool, practical application of MBN techniques has been limited by magnetic coupling issues, which reduce the selectivity of the measurement [3].

Small changes in excitation magnet lift-off produce large changes in the magnetic circuit permeability, and sensor position dramatically affects the sensitivity to the Barkhausen effect. Despite improvements in Barkhausen theory, there has been little improvement in NDE instrumentation.

Most MBN test apparatus employ current control for the excitation coil, as this current is proportional to the applied magnetic field (e.g. [2]). Typically, excitation waveforms are sinusoidal [4–8, 18, 19, 22] or triangular [9–12, 17, 23, 24], at frequencies ranging from 0.005 Hz [4] to 12 Hz [6]. Some researchers monitor both the applied field and the magnetic circuit flux, either by winding coils directly on/around the sample [6, 10, 12, 16–20, 22, 24, 25] or by winding sensing coils on the excitation magnet poles [7].

The requirement of winding a coil on/around the sample to monitor the flux is not practical for use in many geometries and NDE applications in particular. Therefore, in the present work the flux in the excitation magnet poles is monitored. The measured flux is fed back into the excitation magnet waveform to effectively control the magnetic flux coupled into the sample, under a variety of excitation magnet lift-off conditions. The use of this flux-controlled MBN approach for magnetic anisotropy estimation is also investigated.

2. Theory

The Barkhausen effect is measured as sudden changes in the sample magnetization distribution **M**, caused by domain structure reconfiguration around pinning sites. The domain activity is induced by an applied alternating magnetic field **H**. To generate consistent Barkhausen measurements it is necessary that **M**, a time-dependent vector distribution, be reproduced in terms of direction, amplitude and time, for each measurement. A general description of bulk magnetic behaviour in a material is

$$\mathbf{B} = \mu_0 (\mathbf{H} + \mathbf{M}) = \mu_0 \left(\mathbf{1} + \boldsymbol{\chi}_m\right) \mathbf{H} = \mu_0 \boldsymbol{\mu}_r \mathbf{H}, \tag{1}$$

where **B** is the flux density distribution, μ_0 is the permeability of free space, $\boldsymbol{\chi}_m$ is the susceptibility tensor and $\boldsymbol{\mu}_r$ is the relative permeability tensor [2, 26, 27]. If the material is ferromagnetic, then $\boldsymbol{\chi}_m \gg \mathbf{1}$ in regions where MBN primarily occurs [6], and $\mathbf{B} \approx \mu_0 \mathbf{M}$. Therefore, the dominant contribution to flux density distribution in a ferromagnetic material is the sample magnetization distribution, making **B** a suitable control parameter for Barkhausen noise measurements.

A typical surface MBN apparatus, which features a U-core excitation magnet, is shown in figure 1. The circuit is composed of three materials: the core, the sample and the air gap (or any $\boldsymbol{\mu}_r = \mathbf{1}$ material). Assuming that permeabilities are isotropic, and that negligible flux leakage occurs, the circuit can be analysed using the magnetic equivalent of Kirchoff's current law [2] to give the effective circuit permeability μ_e (treated here as a scalar), relating **H** to the sample flux density distribution $\mathbf{B}_s$:

$$\mu_e^{-1} = \mu_c^{-1} \frac{\ell_c}{\ell_{tot}} \frac{A_s}{A_c} + \mu_s^{-1} \frac{\ell_s}{\ell_{tot}} + \frac{\ell_g}{\ell_{tot}} \frac{A_s}{A_c}, \tag{2}$$

where ℓ_c, ℓ_s and ℓ_g are the mean flux path of the core, the sample and the gap respectively, $\ell_{tot} = \ell_c + \ell_s + \ell_g$, μ_c and μ_s are the relative permeabilities of the core and the sample respectively, and A_s/A_c is the ratio of the sample cross section to the core cross section. Given that both $\mu_c \gg 1$ and $\mu_s \gg 1$, equation 2 shows that even a small gap (i.e. $\ell_g/\ell_{tot} > 0$) between the magnet and the sample, such as that caused by coatings or rust, will significantly reduce the circuit permeability, and also reduce $\mathbf{B}_s$ and **M** for a given **H**. In order to induce a specific **M** waveform, which is essential for reproducible MBN results, $\mathbf{B}_s$ must therefore be monitored and controlled.

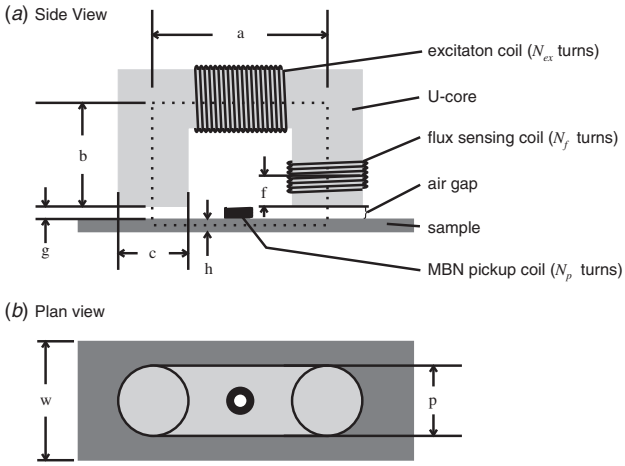

Figure 1. A typical U-core surface magnetic Barkhausen noise probe.

While all the flux in the circuit can be assumed to go through the excitation coil, this flux does not necessarily pass through the sample. The flux coupled from the core into the sample is best measured with an encircling coil; however, this is not possible for most NDE geometries. In an NDE system, the flux should be measured as close as possible to the sample for example by winding a flux-sensing coil at the end of the pole piece as shown in figure 1. According to Faraday's law [2], the voltage (V_f) induced on a coil with N_f turns wound on the pole will be proportional to the rate of change of the total flux ($\dot{\Phi}$) through it:

$$V_f = -N_f \dot{\Phi}. \tag{3}$$

Continuously integrating V_f/N_f with respect to time provides an estimate of the flux Φ coupled into the sample, subject to a constant, which is the flux in the magnetic circuit due to any remnant magnetization. This constant can be assumed to be zero if the circuit is demagnetized prior to MBN testing.

The flux Φ is related to the sample flux density distribution $\mathbf{B}_s$ by the sample area A_s:

$$\Phi = \int \mathbf{B}_s \cdot \mathrm{d}A_s. \tag{4}$$

While the exact $\mathbf{B}_s$ is not known, it is convenient to assume that $\mathbf{B}_s$ is constant for a given circuit geometry and excitation waveform. Under this assumption Φ can be considered proportional to the average $|\mathbf{B}_s|$, related by the effective area of the sample to the magnetic circuit A_s. Since $\mathbf{B}_s$ and A_s differ between magnetic circuit geometries, MBN signals from different geometries are not expected to be consistent.

The sample magnetization is also affected by the excitation frequency as eddy currents induced in the sample

reduce the flux penetration [28]. Since the flux penetration is a function of frequency, various excitation frequencies induce flux at different depths in the sample, creating an inhomogeneous flux distribution, particularly in samples thicker than the skin depth.

While the apparatus in this work does control the circuit flux, the extent to which $\mathbf{M}$ and $\dot{\mathbf{M}}$ are known in the samples is limited by the $\mathbf{B} \approx \mu_0\mathbf{M}$ approximation. Furthermore, with the varying circuit permeability introduced by lift-off, an accurate measure of $\mathbf{H}$ in the sample is not performed. Therefore the MBN signal cannot be discriminated with respect to the differential sample permeability, and the MBN statistics are gathered from the full hysteresis cycle. As such, there is insufficient discrimination to observe the critical behaviour seen in [17–20] and reviewed in [21]. The objective in the present study is to ensure that $\mathbf{M}$ and $\dot{\mathbf{M}}$ are sufficiently reproduced to observe consistent MBN.

In this work we set the excitation frequency to 12 Hz, and vary the excitation waveform amplitude to achieve different peak flux values as well as different flux rates. As the peak flux in the sample increases, there will be an increased magnetization, domain activity and thus MBN, and as the flux rate increases there will be a change in the MBN signal amplitude due to the more rapid magnetization processes. Since both an increased flux and an increased flux rate will result in an increased MBN signal, by choosing a single excitation frequency sinusoid and varying the amplitude, the reported measurements are subject to both effects simultaneously.

The orientation of the excitation magnet on the sample surface is also essential to measurement reproducibility as a result of sample magnetic anisotropy. The domain structure of a sample material may not be uniform as it is affected by material microstructure and thus stress and texture. MBN measurements may be used to estimate the projection of the magnetic anisotropy in the plane of the excitation field, by rotating the excitation magnet about a point on the surface of the sample. Such 'angular MBN' measurements have been used in previous studies for determining both the magnitude and direction of an applied stress, with tensile stresses resulting in an increase in the MBN signal and compressive stresses resulting in a decrease [6–8]. The appropriateness of flux control rather than field control for this type of angular MBN measurement is evaluated in the later sections of this work.

3. Experimental technique

In order to verify magnetic circuit permeability independence, the Barkhausen effect was investigated in two samples with significantly different magnetic properties:

- a 0.50 mm thick sheet of non-grain-oriented Si–Fe steel with no easy axis—to test lift-off independence,
- a 1.6 mm thick interstitial-free (IF) steel sample with a known easy axis [8]—to test lift-off independence along the easy axis and sensitivity to magnetic anisotropy via angular MBN measurements.

Two ferrite core excitation magnets were used: one for lift-off measurements and one for angular MBN measurements. Their dimensions and coil information are given in table 1. For lift-off measurements the assembly was large enough that the magnet could be raised independently of the pickup coil. Plastic spacers 150 ± 2 μm thick were cut and stacked underneath the excitation magnet poles to provide selected amounts of excitation magnet lift-off, while the pickup coil was fixed to the sample with adhesive tape. For angular MBN measurements the excitation magnet was attached to the pickup coil and was small enough to be rotated on the surface of the samples used.

Table 1. Excitation magnet and pickup coil dimensions (all spatial dimensions in mm).

Magnet	Lift-off	Angular
N_{ex}	1100	478
N_f	29	49
N_p	450	500
Pickup ID	2.0	2.0
Pickup OD	4.7	5.0
Core pole shape	Circular	Rectangular
a	45.3	17.2
b	26.8	14.7
c	18.5	7.2
p	18.5	7.1
ℓ_c	98.9	46.6
f	11.5	5.0

Both excitation magnets were controlled by the computer system indicated in figure 2, which is an electrical circuit schematic of the probe shown in figure 1. This system is based upon a National Instruments PCI-6229 DAQ, used both as an arbitrary waveform generator and as an oscilloscope, and a non-inverting LM4701T op-amp with a gain of 3.7. In order to achieve magnetic field or magnetic flux control, feedback algorithms were used to alter the excitation voltage until the target shunt resistor or flux-sensing coil voltage levels were obtained. LabVIEW® 8.0 was used to implement the system. In addition to Barkhausen measurements, hysteresis loops of the magnetic circuit were recorded. These were used to estimate additional magnetic parameters such as the circuit permeability. The various feedback algorithms used to achieve field and flux control are described below.

3.1. Field control

The excitation magnetic field H is defined as

$$H = \frac{N_{ex} I}{\ell}, \tag{5}$$

where N_{ex} is the number of turns in the excitation coil, I is the excitation coil current and ℓ is the mean length of the magnetic flux path in the circuit. Producing a sinusoidal H therefore requires sinusoidal current control. Current was measured by placing a shunt resistor with resistance R_{shunt} in series with the excitation coil, as shown in figure 2. Since the current through the excitation coil is the same as that through the shunt, one can calculate the current using Ohm's law:

$$I = \frac{V_{shunt}}{R_{shunt}}, \tag{6}$$

where V_{shunt} is the voltage across the shunt resistor. Taking into account the excitation inductance L_{ex}, its resistance R_{ex} and R_{shunt}, the total amplified voltage V_{BOP} is

$$V_{BOP} = L_{ex}\frac{dI}{dt} + (R_{ex} + R_{shunt})\, I. \tag{7}$$

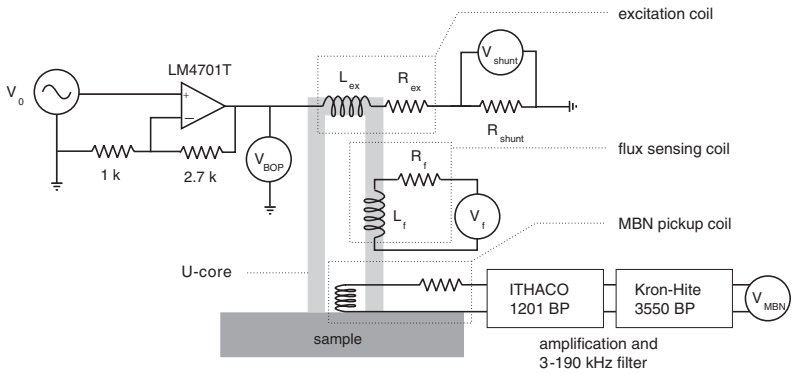

Figure 2. Electrical circuit schematic for the computer-based MBN data acquisition system. All potentials are provided and sampled by the NI PCI-6229 DAQ. Inductive coils are modelled as an ideal inductor and a series resistance. The MBN pickup coil signal is amplified ×2000, and band-pass filtered between 3 kHz and 190 kHz.

To achieve a target current waveform with a specified voltage, an iterative approach was used. The drive voltage of the nth feedback loop $V_{0,n}$ was defined as

$$V_{0,n} = V_{0,n-1} + G\left((I_{\text{targ}} - I_{n-1}) + \frac{L_{\text{ex}}}{R_{\text{ex}} + R_{\text{shunt}}}\frac{\text{d}}{\text{d}t}(I_{\text{targ}} - I_{n-1})\right) \quad (8)$$

where G is the feedback gain, I_{n-1} is the current waveform of the $(n-1)$th loop and I_{targ} is the target current waveform. The ratio of L_{ex} to the total resistance may be calculated or varied until the algorithm is successful. In the present study a value of $L_{\text{ex}}/(R_{\text{ex}} + R_{\text{shunt}}) = 100$ was used.

3.2. Flux control

In order to estimate the magnetic flux coupled into the sample, flux-sensing coils were wound on the poles near the place where they contact the sample, as shown in figure 1. Losses due to coil resistance were expected to be small and were considered negligible. The voltage across the flux sensing coils V_{f} was related to the change in flux through the coils by equation 3. The relative phase of the applied voltage and the feedback voltage was measured by sampling both V_{BOP} and V_{f} simultaneously. An iterative correction to V_{ex} in order to achieve a sinusoidal V_{f} was then applied as follows:

$$V_{0,n} = V_{0,n-1} + G\left(\Phi_{\text{targ}} - \frac{1}{N_{\text{f}}}\int V_{f,n-1}\,\text{d}t\right). \quad (9)$$

In both current and flux control, corrections to the excitation waveform were halted when the absolute average difference between target and measured waveforms was less than 1% of the average absolute target amplitude. Barkhausen measurements were then obtained, using the adjusted excitation waveforms, at the maximum sampling frequency of the DAQ, which is 253 kHz. This sampling rate is below the Nyquist criterion for the MBN signal, which was filtered between 3 kHz and 190 kHz, so there may be some aliasing of higher frequencies in the MBN data. This under-sampling was expected to increase the variance of MBN measurements, and was compensated for by averaging multiple results.

Though a 12 Hz excitation field is too rapid to observe and count individual MBN events, MBN is still observed. To quantify the intensity of the MBN signal in terms of a single value, an $\text{MBN}_{\text{energy}}$ parameter was used as in previous studies [6, 8, 22],

$$\text{MBN}_{\text{energy}} = \frac{1}{T}\int_0^T V^2\,\text{d}t, \quad (10)$$

where V is the MBN signal waveform and T is the period of the excitation field. Only signal voltages greater than a threshold value, determined as three standard deviations from the mean background noise in the pickup coil, were included in the integration. $\text{MBN}_{\text{energy}}$ units are not absolute, as the noise sensed by the pickup coil is subject to the pickup coil geometry, signal amplification and filtering.

4. Results and discussion

Lift-off studies were conducted on both the non-grain oriented Si–Fe and IF steel samples and are presented in section 4.1. Section 4.2 describes the angular MBN measurement studies, conducted only on the IF steel sample (since it displayed considerable magnetic anisotropy).

4.1. Lift-off studies

In this section, lift-off was achieved by placing plastic spacers between the excitation magnet and the sample, while the pickup coil was affixed to the sample with adhesive tape. This procedure produced an air gap under both pole pieces of the excitation magnet, with a total gap length of double the lift-off value indicated. Though the introduction of lift-off changes the permeability of the magnetic circuit, the permeability of the sample should remain constant, provided the orientation of the excitation magnet does not change. The sensitivity to lift-off was studied at a variety of magnetic fluxes as described below.

4.1.1. Non-grain-oriented Si–Fe steel. Examples of the Barkhausen waveforms from the Si–Fe steel sample for peak sample flux densities of 0.54 T and 1.74 T are shown in figures 3(*a*) and (*b*) respectively, where the sample flux density is defined as Φ/A_{s}, with $A_{\text{s}} = p \cdot h$ as shown in figure 1. The sinusoidal feedback coil voltage is also indicated, corresponding to $\dot{\Phi}$.

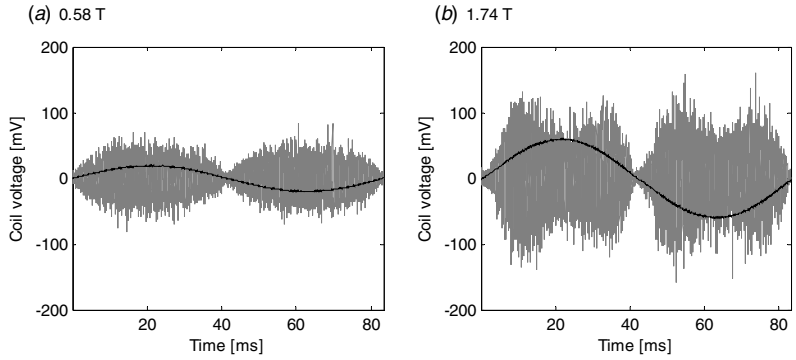

Figure 3. MBN pickup coil (grey) and flux sensing coil (black sinusoid) voltage waveforms in the Si–Fe steel sample, for peak sample flux densities of (*a*) 0.58 T and (*b*) 1.74 T.

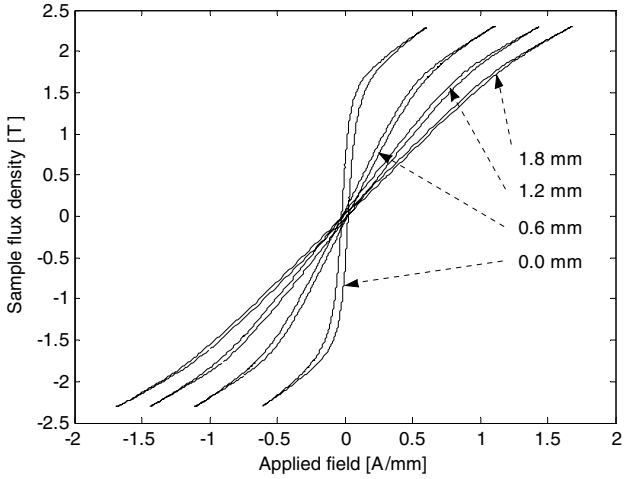

Figure 4. B–H loops for the Si–Fe sample with varying degrees of lift-off as indicated.

To test the MBN signal response to lift-off, $\mathrm{MBN}_{\mathrm{energy}}$ and peak H values were measured at lift-off values of 0.0, 0.6, 1.2 and 1.8 mm with a sinusoidal circuit flux. Each measurement is the average $\mathrm{MBN}_{\mathrm{energy}}$ for 16 excitation cycles at a frequency of 12 Hz. Figure 4 shows the B–H loops for the four lift-off values chosen. Figures 5(*a*) and (*b*) show the $\mathrm{MBN}_{\mathrm{energy}}$ as a function of peak H, and the peak sample flux density Φ/A_{s} respectively. Figure 5(*b*) indicates magnetic saturation at $\Phi/A_{\mathrm{s}} \cong 2$ T and $\mathrm{MBN}_{\mathrm{energy}} \cong 125\ \mathrm{mV}^2\ \mathrm{s\ Hz}$, consistent with the saturation behaviour shown in figure 4 and typical values expected for this material [29], indicating that the circuit flux density is limited by the sample in this case.

Field control. Figure 5(*a*) shows that for measurements performed at constant peak field (a vertical line in the plot), $\mathrm{MBN}_{\mathrm{energy}}$ decreases with progressively increasing lift-off. This implies that in order to maintain a constant $\mathrm{MBN}_{\mathrm{energy}}$, the drive current must be increased with lift-off to compensate for the drop in the magnetic circuit permeability due to the air gap. This decrease in the circuit permeability is verified by the decrease in the hysteresis loop slope as lift-off increases, shown in figure 4.

Flux control. Figure 5(*b*) shows that, for a particular constant peak flux density (a vertical line in the plot), the $\mathrm{MBN}_{\mathrm{energy}}$ is essentially independent of lift-off. The largest $\mathrm{MBN}_{\mathrm{energy}}$ drop, going from 0 mm to 1.8 mm at a flux density of 1.5 T, is less than 10%. When saturation is reached above $\Phi/A_{\mathrm{s}} \cong 2$ T, $\mathrm{MBN}_{\mathrm{energy}}$ values become essentially lift-off independent.

Pulse height distributions. Figure 5(*a*) indicates that MBN measurements performed with a fixed peak applied field are lift-off dependent, while figure 5(*b*) shows that fixed peak flux control significantly reduces the dependence on lift-off. To further investigate the lift-off sensitivity of $\mathrm{MBN}_{\mathrm{energy}}$ under flux control, the MBN pulse height distribution (PHD) was investigated for four peak flux density values and the four lift-off cases considered earlier. For each of 16 excitation cycles, the PHD was calculated as a histogram of the absolute MBN waveform amplitude in each of 128 bins. These 16 PHDs were then averaged to produce the PHDs shown in figure 6, and the associated standard error from this average was computed for each bin.

Figure 6(*a*) shows the PHDs for MBN signals with peak flux densities of 0.58, 1.16, 1.74 and 2.32 T at 0.0 mm lift-off. This figure illustrates the change in MBN statistics with an increase in the magnetization amplitude and rate. Rather than comparing PHDs directly as in figure 6(*a*), a quantitative measure of consistency between the PHDs is obtained by subtracting the PHDs and plotting the difference, normalized by the error on the subtracted bin values, σ. As an example, figure 6(*b*) shows the differences between the 2.32 T data in figure 6(*a*) and that of the 0.58, 1.16 and 1.74 T data. With typical deviations on the order of 10 σ to 60 σ, MBN data collected at various peak flux densities are clearly inconsistent. The noise threshold value[3] is shown to indicate the pulse height values that are discarded in the $\mathrm{MBN}_{\mathrm{energy}}$ analysis. Figure 6(*b*) shows that as the flux density is decreased from 2.32 T, the average pulse height decreases above the threshold value, and the number of events that are indistinguishable from the background noise increases.

Figures 7(*a*) and (*b*) indicate, for peak flux densities of 0.58 T and 1.74 T respectively, the PHD differences between 0.6 and 1.8 mm lift-off values compared to 0.0 mm lift-off. As lift-off increases the result is similar to the behaviour

[3] The threshold is three standard deviations from the mean background noise in the pickup coil.

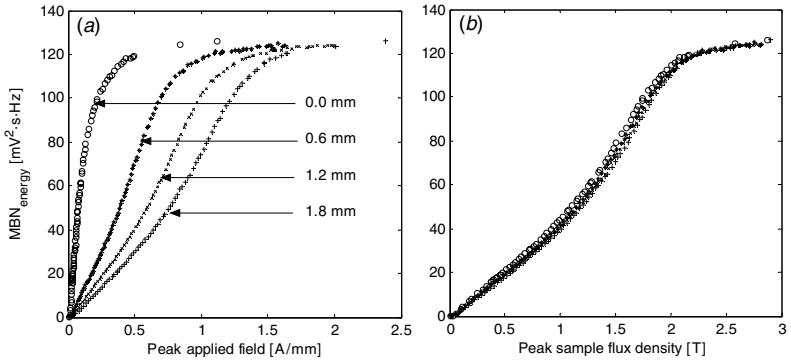

Figure 5. MBN$_{energy}$ lift-off response as a function of the (*a*) peak applied field and (*b*) peak sample flux density for the Si–Fe steel sample.

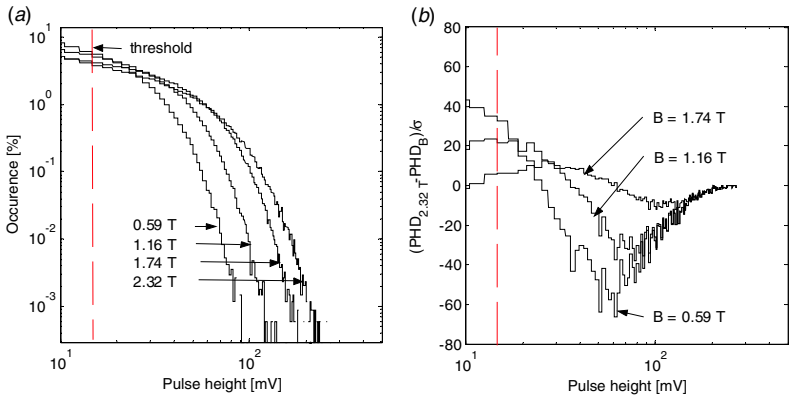

Figure 6. (*a*) MBN signal PHDs in Si–Fe steel due to a 12 Hz sinusoidal flux excitation waveform with peak sample flux densities of 0.59, 1.16, 1.74 and 2.32 T. Each PHD was calculated the average absolute pulse height in 128 bins over 16 excitation cycles. (*b*) The differences between the PHD for 2.32 T and the PHDs for 0.59, 1.16 and 1.74 T, normalized by the standard error on the difference for each bin.

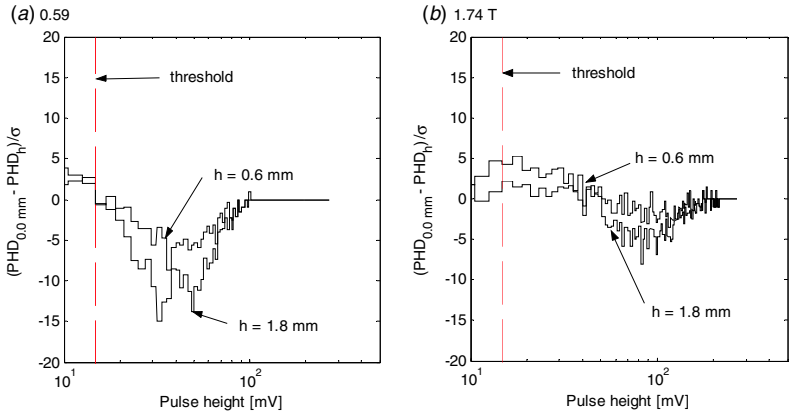

Figure 7. Differences between MBN PHDs with 0.0 mm lift-off and PHDs with the indicated lift-off values, normalized by the error on the difference, in the Si–Fe steel sample for peak sample flux densities of (*a*) 0.59 T and (*b*) 1.74 T.

observed in figure 6(*b*), indicating a decrease in the sample flux density with increasing lift-off. This may be attributed to the approximation that the flux in the sample is assumed equal to the flux through the poles. It is expected that with increasing lift-off some portion of the flux passing through the feedback coil may connect directly between the poles and not enter the sample. Placing the feedback coil as close as possible to the end of the pole (reducing 'f' in figure 1) is expected to reduce this error, and thus is a design consideration when winding excitation magnets.

Comparing figures 7(*a*) and (*b*) indicates that the lift-off differences are smaller for the higher peak flux density of figure 7(*b*). Table 2 includes the absolute mean and standard deviation of the PHD differences for 0.58, 1.16, 1.74 and 2.32 T. A value less than 2 indicates that the average PHD at the specified flux and lift-off is within two standard error values of the PHD at that same flux with no lift-off. The data in table 2 therefore indicate that flux control may be considered to yield lift-off independent results within a 95% confidence level for lift-off values 0.6 mm or less at flux densities of

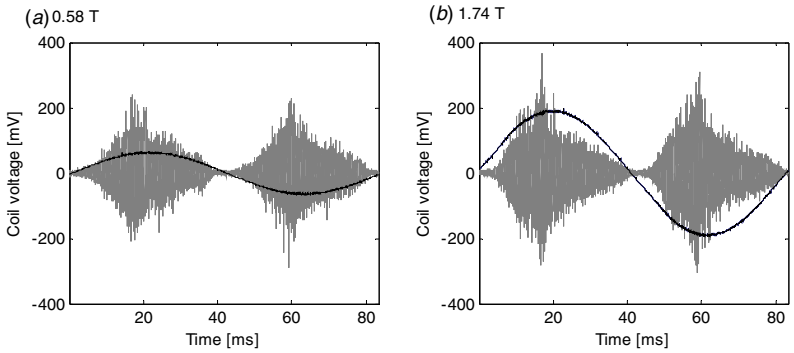

Figure 8. MBN pickup coil (grey) and flux sensing coil (black sinusoid) voltage waveforms in the IF steel sample along the easy axis, for peak sample flux densities of (*a*) 0.58 T and (*b*) 1.74 T.

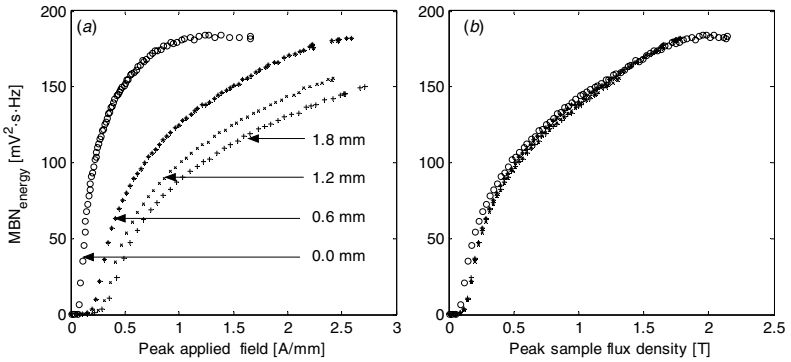

Figure 9. MBN_{energy} lift-off response as a function of the (*a*) peak applied field and (*b*) peak applied flux density for the IF steel sample along the easy axis.

Table 2. Consistency of pulse-height distributions under lift-off at a variety of flux densities and lift-off values in the Si–Fe steel sample.

Lift-off h (mm)	Absolute average pulse-height consistency with 0.0 mm lift-off case above the background noise threshold $\overline{\lvert PHD_{0.0mm} - PHD_h \rvert}/\sigma$			
	0.58 T	1.16 T	1.74 T	2.32 T
0.6	3.3 ± 2.0	1.21 ± 0.84	1.24 ± 0.79	1.02 ± 0.75
1.2	4.1 ± 2.6	2.0 ± 1.4	1.7 ± 1.1	1.08 ± 0.86
1.8	6.4 ± 4.3	3.2 ± 2.0	2.8 ± 1.7	1.4 ± 1.1

1.16 T or more, with increasing independence from lift-off as the flux density increases.

4.1.2. IF steel along the easy axis direction. Sample Barkhausen waveforms from the IF steel sample for peak flux densities of 0.29 T and 1.74 T are shown in figures 8(*a*) and (*b*) respectively. The envelope of the MBN signals is different from those shown in figure 3, indicating the significantly different domain structure of the IF sample.

In figures 9(*a*) and (*b*) the MBN_{energy} along the easy axis is shown as a function of the peak applied field and peak flux density respectively. The lift-off sensitivity of field control due to circuit permeability changes is again observed in figure 9(*a*). In figure 9(*b*), the MBN_{energy} as a function of the peak sample flux density is nearly independent of lift-off, as was the case for the non-grain oriented Si–Fe sample.

PHD analysis similar to that for the Si–Fe sample was also performed on the IF steel sample. The results are not shown, but also support the explanation that some flux leakage with increasing lift-off occurs. PHD differences are indicated in table 3. For the IF steel, at 0.29 T and 0.6 mm lift-off the PHDs were consistent. Above 0.58 T, all PHDs were consistent for all lift-off values used, within a 95% confidence level. This indicates that at 0.29 T or higher, a lift-off of 0.6 mm or less can be accommodated by flux control, with additional improved accommodation to lift-off at higher flux densities.

4.2. Angular MBN measurements

As the domain structure affects all magnetic properties of the material, a sample with magnetic anisotropy will also have anisotropic permeability [2]. It is expected that a flux control method will have a different sensitivity to the anisotropy when compared to a field control method, since angular variation in the sample permeability will affect the **M** achieved for a given applied **H**, but **M** will be approximately constant in the direction of the applied field under an applied Φ. A comparison of angular MBN measurements under flux and

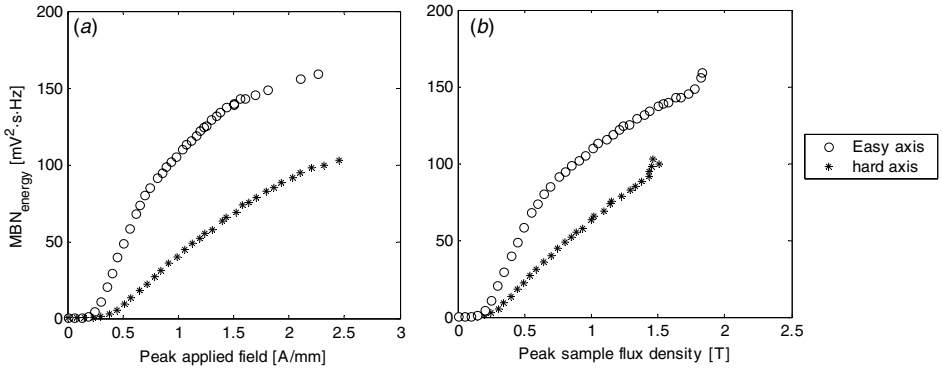

Figure 10. MBN_{energy} response as a function of the (*a*) peak applied field and (*b*) peak sample flux density for the IF steel sample along the easy axis and hard axes at a constant lift-off of 0.5 mm.

Table 3. Consistency of pulse-height distributions under lift-off at a variety of fluxes and lift-off values in the IF steel sample along the easy axis.

Lift-off h (mm)	Absolute average pulse-height consistency with 0.0 mm lift-off case above the background noise threshold $\overline{\lvert PHD_{0.0mm} - PHD_h \rvert}/\sigma$			
	0.29 T	0.58 T	1.16 T	1.74 T
0.6	1.24 ± 0.80	0.75 ± 0.63	0.88 ± 0.58	0.84 ± 0.73
1.2	2.1 ± 1.2	1.04 ± 0.80	0.86 ± 0.61	
1.8	2.6 ± 1.3	1.25 ± 0.74	0.97 ± 0.70	

current control was performed on the IF steel sample[4] to answer two questions:

(1) under constant field control, how much of the MBN anisotropy is due to a simple permeability relationship between the **H** applied and the **M** achieved?
(2) Under constant flux control, and therefore constant **M** in the direction of the applied field, how much of the MBN anisotropy is due to domain structure anisotropy?

Figures 10(*a*) and (*b*) show the MBN_{energy} response as a function of peak H and Φ/A_s respectively, along the easy and hard axis of the IF steel sample, with a constant lift-off of 0.5 mm. The plots show that for both constant peak field and constant peak sample flux density (which would be represented by a vertical line on either figures 10(*a*) or (*b*)) there is a significant difference in the MBN_{energy} observed between the hard and easy axes. The upturning behaviour at the highest flux densities in figure 10(*b*) is attributed to magnetic circuit saturation effects.

Since figure 10(*b*) demonstrates a considerable difference between the hard and easy axis, it can be concluded that constant flux measurements may indeed be used to measure the magnetic anisotropy. The particular component of the anisotropy measured using flux control corresponds to the differing domain structure and magnetization processes along the hard and easy axis. From purely geometrical arguments, the pickup coil is roughly twice as sensitive to 180° domain wall motion as it is to 90° domain wall motion and domain rotation. Hence, it is expected that along the hard axis there is a lower population of 180° domain walls, and an increase in magnetization processes that feature the 90°motion and rotation that the pickup coil is less sensitive to.

[4] Significant anisotropy is not present in the Si-Fe sample.

Angular MBN_{energy} measurements of the IF sample are shown in figure 11, both under field control and flux control. The two types of control were 'normalized' so that each produced the same MBN_{energy} along the easy axis direction for three cases, corresponding to peak sample flux densities of 0.5 T, 1.0 T and 1.5 T. The orientation of the excitation magnet was then varied in 10° or 15° increments, and at each angle, the MBN_{energy} was measured for the specified constant peak field and constant peak flux density.

At all field and flux density levels shown in figures 10 and 11 the MBN angular anisotropy is larger under field control than under flux control. The hysteresis loops along the hard and easy axes are shown in figure 12, and their slopes indicate that the permeability of the hard axis is less than that of the easy axis. A constant peak field set to achieve a specific magnetization on the easy axis therefore achieves a lower magnetization on the hard axis and a correspondingly lower MBN_{energy}, as less domain activity is required to produce the lower magnetization. Since MBN anisotropy measurements made at constant peak sample flux density require that the magnetization be achieved regardless of the circuit permeability, there is more domain activity along the hard axis than in the constant peak field case, and hence a relatively higher MBN_{energy} is measured.

4.3. Implications for NDE

In terms of strain and stress characterization, the MBN anisotropy and its strain sensitivity are the parameters of interest [8, 30]. While the data indicate that flux-controlled MBN measurements are less sensitive to the magnetic anisotropy in general, it must be noted that the anisotropy measured at constant peak flux is nearly independent of the permeability of the magnetic circuit. Flux-controlled

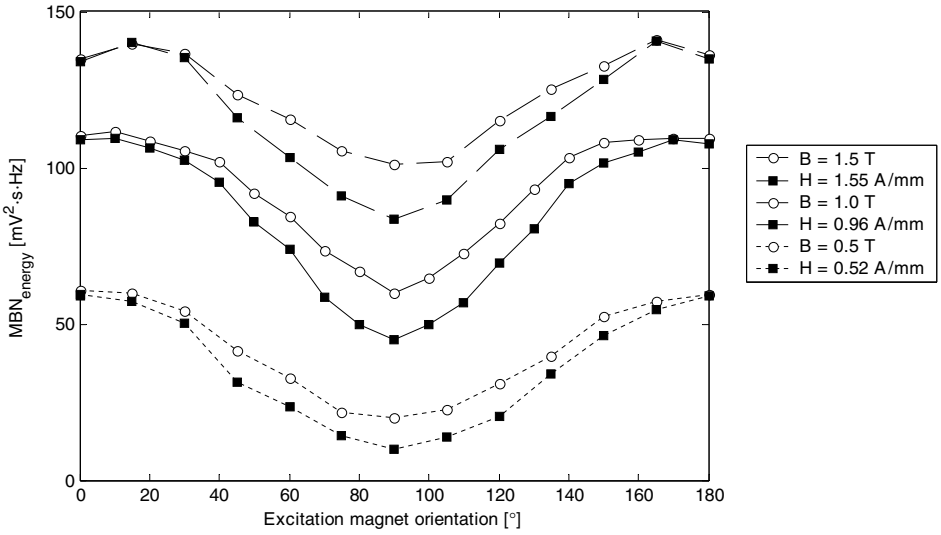

Figure 11. Constant peak sample flux density and constant peak field angular MBN measurements on the IF steel sample with peak sample fluxes along the easy axis of 0.5, 1.0 and 1.5 T. 0° corresponds to the known easy axis direction of the sample. Data are connected to guide the eye.

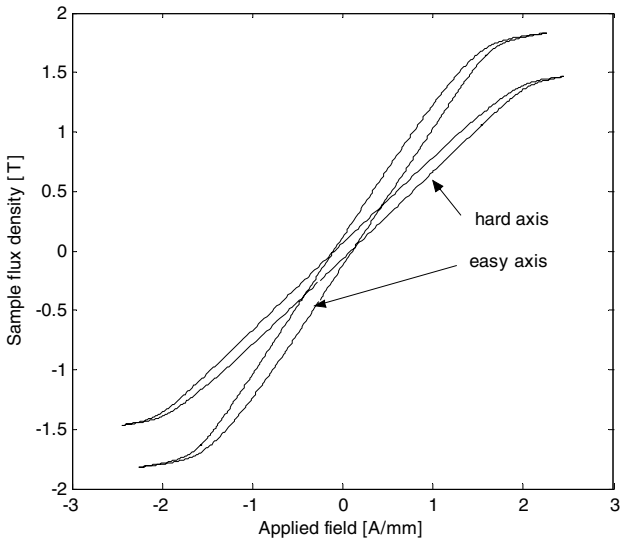

Figure 12. B–H loops for the IF steel sample along the hard and easy axes using the angular excitation magnet.

measurements are minimally affected by lift-off as compared to field-controlled measurements, as demonstrated in the lift-off analysis. Furthermore, the degree to which the anisotropy sensitivity is increased with field control will vary depending on all factors that affect the circuit permeability including core material and the circuit length. While testing an unknown sample, variances in circuit permeability could be due to a number of factors, excluding the magnetic anisotropy, which must be accounted for when performing field-controlled measurements.

The independence of flux-controlled MBN measurements to magnetic circuit permeability is desirable for NDE applications of the Barkhausen effect, as it will allow more reproducible measurements on samples with irregular surface geometries and coatings. This work did not address the effects of pickup coil lift-off, which will strongly affect the Barkhausen signal observed due to the high frequency and small skin depth of Barkhausen events. However, within the two-component system, eliminating contact issues within the excitation circuit is the first step towards a more robust measurement system.

Furthermore, the principle of controlling the circuit flux directly with feedback methods should be of interest to any NDE technique relying on inducing flux into samples to produce a signal. For example, application of such feedback to electromagnet-based magnetic flux leakage studies would eliminate the need for current calibration, as the flux would be directly controlled.

4.4. General implications for Barkhausen noise measurements

In general this experiment demonstrates that controlling the flux in a surface MBN circuit is an effective means of reproducing the sample magnetization conditions. While this study employed sinusoidal flux waveforms, the experimental setup allows control of arbitrary periodic flux waveforms.

For fundamental studies, if the feedback coil were wound around the sample as opposed to the core, then the bulk sample magnetization could be directly controlled without approximation. For example, if a triangular flux waveform were chosen and the frequency were altered to maintain a constant flux rate, it would be possible to examine MBN at any position on the hysteresis loop and gather a complete statistical description of MBN with respect to $\mathbf{M}$, $\dot{\mathbf{M}}$ and $\mathbf{H}$.

While only major hysteresis loops are explored with a purely ac waveform, it would also be possible to explore minor hysteresis loops in special geometries by doing similar flux control with a dc current offset. This type of experiment would allow MBN statistics to be studied at near-saturation flux levels where domain creation and annihilation processes, as well as domain rotation processes, are taking place.

5. Summary

It was demonstrated that the magnetic flux coupled into the sample can be estimated from the voltage on coils wound on U-core excitation magnet poles near the sample, and that appropriately adjusting the excitation coil waveform can be used to control this flux. The sensitivity of surface Barkhausen noise measurements to changes in magnetic circuit permeability was investigated for sinusoidal magnetic field and magnetic flux control on a non-oriented Si–Fe electrical steel and an IF steel sample.

Circuit permeability was varied by changing the lift-off of the excitation magnet and by using a sample with known MBN anisotropy. It was demonstrated that while MBN_{energy} measurements performed at a constant peak field varied strongly with the circuit permeability, MBN_{energy} measurements with constant peak flux were nearly consistent over the entire range of flux density achievable in the samples. Specifically, for the Si–Fe samples, MBN signals were consistent for lift-off values of 0.6 mm or less at flux densities of 1.16 T or more. For the IF steel sample along the easy axis, MBN signals were consistent for lift-off values 0.6 mm or less at all flux densities higher than 0.29 T.

In the magnetically anisotropic IF steel sample it was shown that the degree of anisotropy measured under flux control was independent of the magnetic circuit permeability, but that the anisotropy was not independent under field control. Field control results were more sensitive to magnetic anisotropy, but a component of this sensitivity is essentially an artefact due to the lower magnetization achieved along the hard axis of the sample. While in this case the decrease in permeability along the hard axis was known to be due to magnetic anisotropy, in general this cannot be assumed.

It is recommended that future MBN measurements include time-based monitoring of the sample flux density, and are reported in terms of the sample flux density or magnetization rather than the applied magnetic field. MBN measurements will only be consistent and comparable provided that the sample magnetization distribution is achieved in the same manner for each measurement, and controlling the circuit flux density is an effective means of achieving this goal.

References

[1] Alessandro B, Beatrice C, Bertotti G and Montorsi A 1988 Phenomenology and interpretation of the Barkhausen effect in ferromagnetic materials (invited) *J. Appl. Phys.* **64** 5355–60

[2] Cullity B D 1972 *Introduction to Magnetic Materials* vol 22 (Reading, MA: Addison-Wesley) pp 69–71

[3] Lo C C H 2004 A review of the Barkhausen effect and its applications to nondestructive testing *Mater. Eval.* **62** 741–8

[4] Grum J and Zerovnik P 2000 Use of the Barkhausen effect in the measurement of residual stresses in steel *Insight* **42**

[5] Rautioaho R, Karjalainen P and Moilanen M 1987 Stress response of Barkhausen noise in a tempered C–Mn steel *J. Magn. Magn. Mater.* **68** 314–20

[6] Krause T, Makar J M and Atherton D L 1994 Investigation of the magnetic field and stress dependence of 180° domain wall motion in pipeline steel using magnetic Barkhausen noise *J. Magn. Magn. Mater.* **137** 25–34

[7] Vengrinovich V L and Tsukerman V L 2004 Stress and texture measurement using Barkhausen noise and angular scanning of driving magnetic field *16th WCNDT 2004 World Conference on NDT (Montreal)*

[8] Hutanu R 2004 A correlation study between magnetic Barkhausen noise and intergranular residual stresses in steels *PhD Thesis* Queen's University, Kingston, Ontario, Canada

[9] Buttle D J, Scruby C B, Briggs G A D and Jakubovics J P 1987 The measurement of stress in steels of varying microstructure by magnetoacoustic and Barkhausen emission *Proc. R. Soc. Lond.* A **414** 469–97

[10] Jiles D C 1989 The Effect of stress on magnetic Barkhausen activity in ferromagnetic steels *IEEE Trans. Magn.* **23** 3455–7

[11] Sablik M J and Augustyniak B 1996 The effect of mechanical stress on a Barkhausen noise signal integrated across a cycle of ramped field *J. Appl. Phys.* **79** 963–72

[12] Jagadish C, Clapham L and Atherton D L 1990 The effect of stress and magnetic field orientation on surface Barkhausen noise in pipeline steel *IEEE Trans. Magn.* **26** 262–5

[13] Tiitto S I 1978 On the mechanism of magnetization transitions in steel *IEEE Trans. Magn.* **14** 527–9

[14] Titto K 1989 Use of Barkhausen effect in testing for residual stresses and material defects *Non-Destr. Test.—Aust.* **26** 36–41

[15] Sundström O and Törrönen K 1979 The use of Barkhausen noise analysis in nondestructive testing *Mater. Eval.* **37** 51–6

[16] Bertotti G, Fiorillo F and Sassi M P 1981 Barkhausen noise and domain structure dynamics in Si–Fe at different points of the magnetization curve *J. Magn. Magn. Mater.* **23** 136–48

[17] Alessandro B, Beatrice C, Bertotti G and Montorsi A 1990 Domain-wall dynamics and Barkhausen effect in metallic ferromagnetic materials: II. Experiments *J. Appl. Phys.* **68** 2908–15

[18] Cote P J and Meisel L V 1991 Self-organized criticality and the Barkhausen effect *Phys. Rev. Lett.* **67** 1334–7

[19] Spasojević D, Bukvić S, Milošević S and Eugene Stanley H 1996 Barkhausen noise: elementary signals, power laws, and scaling relations *Phys. Rev.* E **54** 2531–46

[20] Tadić B 1999 Dynamic criticality in driven disordered systems: role of depinning and driving rate in Barkhausen noise *Physica* A **270** 125–34

[21] Durin G and Zapperi S 2004 The Barkhausen effect *Preprint* cond-mat/0404512

[22] Krause T, Clapham L and Atherton D L 1994 Characterization of the magnetic easy axis in pipeline steel using magnetic Barkhausen noise *J. Appl. Phys.* **75-12** 7983–8

[23] Zhu B, Johnson M J, Lo C C H and Jiles D C 2001 Multifunctional magnetic Barkhausen emission measurement system *IEEE Trans. Magn.* **37** 1095–9

[24] Clapham L, Jagadish C, Atherton D L and Boyd J D 1991 The influence of controlled rolling on the pulse height distribution of magnetic Barkhausen noise in steel *Mater. Sci. Eng.* A **145** 233–41

[25] Jiles D C 1988 Integrated on-line instrumentation for simultaneous automated measurement of magnetic field, induction, Barkhausen effect, magnetoacoustic emission and magnetostriction *J. Appl. Phys.* **63** 3946–8

[26] Yu Y, Krause T W, Weyman P and Atherton D L 1997 Tensor magnetic hysteresis loop measurements of a steel cube *J. Magn. Magn. Mater.* **166** 290–6

[27] Griffiths D J 1999 *Introduction to Electrodynamics* 3rd edn (Upper Saddle River, NJ: Prentice-Hall)

[28] Cheng D K 1992 *Field and Wave Electromagnetics* 2nd edn (Reading, MA: Addison-Wesley)

[29] Bozorth R M 1951 *Ferromagnetism* ed D Van Nostrand (Princeton, NJ: Princeton University Press)

[30] Mandache C 2004 Magnetic flux leakage investigation of interacting defects—stress and geometry effects *PhD thesis* Queen's University, Kingston, Ontario, Canada